

Dynamic density functional theory of protein adsorption on polymer-coated nanoparticles

Stefano Angioletti-Uberti,^{*a,b,c} Matthias Ballauff,^{b,c} and Joachim Dzubiella^{b,c}

Received Xth XXXXXXXXXXXX 20XX, Accepted Xth XXXXXXXXXXXX 20XX

First published on the web Xth XXXXXXXXXXXX 200X

DOI: 10.1039/b000000x

We present a theoretical model for the description of the adsorption kinetics of globular proteins onto charged core-shell microgel particles based on Dynamic Density Functional Theory (DDFT). This model builds on a previous description of protein adsorption thermodynamics [Yigit *et al.*, *Langmuir* 28 (2012)], shown to well interpret the available calorimetric experimental data of binding isotherms. In practice, a spatially-dependent free-energy functional including the same physical interactions is built, and used to study the kinetics via a generalised diffusion equation. To test this model, we apply it to the case study of Lysozyme adsorption on PNIPAM coated nanoparticles, and show that the dynamics obtained within DDFT is consistent with that extrapolated from experiments. We also perform a systematic study of the effect of various parameters in our model, and investigate the loading dynamics as a function of proteins' valence and hydrophobic adsorption energy, as well as their concentration and that of the nanoparticles. Although we concentrated here on the case of adsorption for a single protein type, the model's generality allows to study multi-component system, providing a reliable instrument for future studies of competitive and cooperative adsorption effects often encountered in protein adsorption experiments.

1 Introduction

Protein adsorption on various materials is a fascinating problem with important repercussions for the development of a large number of diverse technologies. These include food manufacturing processes, biomaterials for medical implants and functionalised nanoparticles for targeted drug delivery, among many others¹. The need to understand protein adsorption arises from the fact that the characteristics of the protein layer formed upon adsorption (often called the “protein corona” in the case of nanoparticles), dictates the subsequent interaction of the material with biological entities, for example bacteria, antibodies or cells^{2,3}. Hence, depending on the type of application, one would typically either prevent protein sorption altogether or to allow for some selectivity in the process. In this regard, polymer coatings have been shown to represent a viable way to control protein adsorption, and their intense study gave rise to a vast literature which would be impractical to recapitulate here. The interested reader is referred to a very recent review of the subject by Haag *et al.*⁴, whereas here we will only briefly discuss previous theoretical approaches aimed at describing protein adsorption kinetics.

From a theoretical point of view, protein adsorption kinet-

ics has been mainly studied based on three different approaches: ideal diffusion equations⁵, Langmuir-type models (also called mass-balance equations)^{6,7}, and models based on a “generalised diffusion approach”, also termed “molecular approach”^{8–11}. Given their very nature, models based on *ideal* diffusion cannot capture the complex dynamics of protein adsorption since all the important interactions between proteins and their environment are completely neglected. For this reason, these models do not reproduce at long timescales the right thermodynamics, which is a crucial ingredient to obtain the kinetics, as well as for physical consistency. In fact, as we will show later, calculations based on ideal diffusion produce loading timescales estimates which can be off by two orders of magnitude from those deduced from experiments, although fortuitous cancellation of errors can sometime occur partially correcting the problem in certain cases (see Sec. 3.1). For this reason, care should be taken to avoid over-interpretation of experimental observations based on these simple theoretical description, in particular regarding the proteins' mobility⁵. Despite this caveat, not only protein adsorption but also drug loading and release dynamics onto and from nanoparticles have been typically discussed based on these simple models^{12,13}.

Langmuir models by construction give the correct thermodynamics of protein adsorption. This is often sufficient to correctly reproduce the observed dynamics when single-type protein adsorption occurs and adsorption relies on the Langmuir picture of independent, single binding sites without collective

^{aa} E-mail: sangiolo@physik.hu-berlin.de

^a Institut für Physik, Humboldt-Universität zu Berlin, 12489 Berlin, Germany;

^b Soft Matter and Functional Materials, Helmholtz Zentrum Berlin, 14109 Berlin, Germany

or cooperative effects. However, when multiple protein types coexist, it is hard to guess *a priori* the validity of these assumptions or whether more complex interactions occur. For example, mutual interactions between proteins can induce cooperative adsorption that cannot be casted in terms of single, independent binding sites. Quite generally, it is not possible to say if intermediate, metastable adsorption states observed in protein adsorption, are correctly described by these models. Finally, one important information one would like to have access to is the full density profile as a function of time, not just the amount of adsorbed protein as in a Langmuir model. These profiles can be highly inhomogeneous, in particular for multiple-component systems, and vary strongly in time. Since it is the outer protein shell in contact with the biological environment that determines a nanoparticle's interaction, a correct description of such inhomogeneities is important to understand its functional behaviour. For these reasons, we choose to use a general microscopic approach, as pioneered by Szeleifer and coworkers, who built several models to study protein adsorption for various types of both coated and bare infinite planar surfaces^{8–11}. Our model is similar to the latter in the sense that we start from the same theoretical framework, i.e. Dynamic Density Function Theory (DDFT). However, apart from studying protein adsorption on curved, finite systems like nanoparticles rather than planar surfaces, we will combine DDFT with a different free-energy functional. The latter was inspired by the work of Yigit *et al.*¹⁴ who proposed a coarse-grained model that was shown to well described the protein adsorption for our system. In particular, it included electrostatic cooperativity effects due to the changing net charge of the hydrogel by increasing protein adsorption. Furthermore, it demonstrated that Langmuir models are equivalent to more general description in terms of excluded volume packing effects in the limit of low protein packing fractions in the gel. The latter finding relieves us from the assumption of independent, single binding sites and allows us to describe protein adsorption (especially of multicomponent mixtures) in a more versatile way based on packing effects. As in Ref.¹⁴, we include here the electrostatic contributions within an effective description based on the concept of the Donnan potential. The advantage of this treatment allow us to clearly separate *global* electrostatic effects from *specific*, i.e. protein-dependent ones, shedding some light on the magnitude and relative importance of each of them in different scenarios.

The remaining of the paper is structured as follows. In Sec. 2 we first give a brief, heuristic introduction to the basic DDFT equations, and then proceed to explain the details of our model trying to clearly state all its underlying assumptions and their validity. In Sec. 3, before we proceed to describe the DDFT results, we discuss two analytically solvable models based on the ideal diffusion equation to obtain a first, rough estimate of the timescales expected to appear in our system. Sec. 4 reports

our numerical results for the case of Lysozyme adsorption on PNIPAM coated nanogels, and compare them to extrapolation from the available experimental data as well as those obtained from the solution of the ideal diffusion equation for the same system. We also report a systematic analysis of the role of various interactions and parameters of our model, and critically discuss the obtained results. Finally, we draw our conclusion in Sec. 5.

2 Theoretical Model

2.1 A short introduction to DDFT

At its root, DDFT is nothing but a generalised diffusion equation describing the density evolution of out-of-equilibrium systems undergoing Brownian dynamics^{15–18}. Although a formal derivation starting from the Smoluchowski equation can be built^{15,19}, a less rigorous but more intuitive heuristic argument can be given²⁰, which we will outline here for simplicity. We start with the continuity equation:

$$\frac{\partial \rho_p}{\partial t} = -\nabla \cdot \mathbf{J}_p \quad (1)$$

where $\rho_p(\mathbf{x}, t)$ is the space and time-dependent density field of specie p and \mathbf{J}_p (also a function of time and space) its associated flux. We *assume* \mathbf{J}_p to be linear in the gradient of the chemical potential of the same specie, μ_p , scaled by the inverse temperature $\beta = 1/k_B T$ (where T is the absolute temperature and k_B is Boltzmann's constant), i.e. formally:

$$\mathbf{J}_p(\mathbf{x}, t) = -D_p(\mathbf{x}) \rho_p(\mathbf{x}, t) \nabla \beta \mu(\mathbf{x}, t). \quad (2)$$

The linearity coefficient in Eq. 2 is nothing but the diffusion coefficient D_p . Plugging Eq. 2 into Eq. 1 we obtain a "generalised diffusion equation"

$$\frac{\partial \rho_p}{\partial t} = \nabla \cdot D_p \rho_p \nabla \beta \mu_p \quad (3)$$

which can be written in a more insightful form by splitting the chemical potential into ideal and excess contribution, μ^{id} and μ^{exc} , giving:

$$\begin{aligned} \frac{\partial \rho_p}{\partial t} &= \nabla \cdot D_p \left[\beta \mu_p^{id} + \beta \mu_p^{exc} \right] \\ &= \nabla \cdot D_p \nabla \rho_p + \nabla \cdot D_p \nabla \beta \mu_p^{exc}, \end{aligned} \quad (4)$$

where in the last line we have made the substitution $\beta \mu_p^{id} = \log \rho_p / \rho_0$, ρ_0 being a reference density which we fix to the standard molar density of 1 M. The first term on the r.h.s of Eq. 4 is the ideal diffusion term, which tends to smoothen any

possible density gradient within the system. If no inter-particle interactions nor any external field were present, the excess term would be zero. With the additional constraint of a constant diffusion coefficient D_p , one would then recover the well known formula $\frac{\partial \rho_p}{\partial t} = D_p \nabla^2 \rho_p$, i.e. the ideal diffusion equation. In the general, more realistic case, $\mu^{ex} \neq 0$ and we need a way to calculate this term to determine the dynamical behaviour of the system.

This is provided by classical, equilibrium DFT^{21,22}, which gives the following expression for the chemical potential:

$$\mu_p = \frac{\delta \mathcal{F}[\{\rho_p\}]}{\delta \rho_p}, \quad (5)$$

where $\mathcal{F}[\{\rho_p\}]$ is the free-energy functional of our system, which depends on the densities of all species (labelled by the subscript p).

The underlying assumption at the basis of DDFT is that Eq. 5, remains valid also out of equilibrium, i.e. one is under quasi-equilibrium conditions. A quasi-equilibrium assumption is already implicit in writing Eq. 2 as the gradient of a chemical potential, implying the presence of a conservative field, whereas under full non-equilibrium conditions the true force might be non-conservative. For our specific system, this requires that all other degrees of freedom like the density field of ions and solvent molecules quickly relax around the instantaneous "equilibrium" configuration of the protein density. Moreover, the frequency of external time-dependent fields should not be comparable to the typical relaxation frequency of the system. In these latter scenarios, more complex theories have to be used, such as the recently developed Power Functional Theory of Schmidt and Brader^{23,24}.

When the underlying approximations are met, the agreement between theory and experiments or numerical Brownian dynamics simulations is excellent. In this regard, DDFT has proven to be a versatile instrument, allowing to describe a large variety of phenomena, ranging from the sedimentation of colloids under gravity²⁵⁻²⁷ and colloidal dynamics in polymers mixture²⁸ to the dewetting of evaporating nanoparticle films²⁹, or the kinetics of colloids diffusing in confined geometries^{30,31}. As we are about to show in the later sections, protein adsorption kinetics on polymer-coated charged nanoparticles also appears to be treatable within this framework.

2.2 A free-energy functional for protein adsorption on charged nanogels

As implied by Eq. 5, in order to treat our problem using DDFT we need to specify the free-energy functional for our system

$\mathcal{F}[\{\rho_p\}]$. In its most general form, for any classical system \mathcal{F} can be written as :

$$\begin{aligned} \mathcal{F} &= \mathcal{F}[\{\rho_p\}] = \mathcal{F}^{id} + \mathcal{F}^{ext} + \mathcal{F}^{exc} \\ &= \sum_p \int_V k_B T \rho_p(\mathbf{x}) \left[\ln \left(\frac{\rho_p(\mathbf{x})}{\rho_0} - 1 \right) \right] d\mathbf{x} + \\ &\quad \sum_p \int_V V^{ext} \rho_p(\mathbf{x}) d\mathbf{x} + \mathcal{F}^{exc}[\{\rho_p(\mathbf{x})\}]. \end{aligned} \quad (6)$$

where the sum is over all p species and the integral has to be read as a three-dimensional integral over the whole volume V . Although we will not always make it explicit in the notation, it should be reminded that ρ_p and all other quantities depending on it are both space *and* time-dependent quantities. The first term in Eq. 6 is the free-energy density for an ideal gas of particles, the second describes the coupling between the density and an external potential V^{ext} and the third, typically called the *excess* functional, describes inter-particles interactions.

No *exact* form exists for \mathcal{F}^{exc} , hence Eq. 6 just shifts the problem from the definition of \mathcal{F} to that of \mathcal{F}^{exc} . However, one should notice that in many cases not only most of the free-energy contribution is accounted for by the first two terms, but also that a few useful approximations exist for \mathcal{F}^{exc} , depending on the type of system under consideration. Among these approximations, the simplest possible one, which will also be employed here, is the so-called Local Density Approximation (LDA). In the LDA, one assumes that the excess free-energy density per particle at a point \mathbf{x} is a function of the local density at \mathbf{x} only, and equal to its value for an homogeneous system at the same density, $\epsilon^{exc}(\{\rho_p\})$, i.e.

$$\mathcal{F}^{exc} = \sum_p \int_V \epsilon^{exc}(\{\rho_p(\mathbf{x})\}) \rho_p(\mathbf{x}) d\mathbf{x}. \quad (7)$$

If density fluctuations occur on a scale that is large compared to the interaction range of the particles, each of them "feels" around it an homogeneous environment, and the system should be well described by the LDA. When this is not the case, one can resort to more complex non-local functionals, e.g. those based on a mean-field^{22,32} or "weighted density" approximation³³.

The crucial step in defining our model for protein adsorption is the correct description of the important physical forces that play a role in the adsorption process. In practice, this translates into finding a good approximation for the free-energy functional $\mathcal{F}[\{\rho\}]$. In doing so, we will keep in mind that an important quality we would like to endow our functional with is to contain only experimentally accessible quantities. This latter property will allow us to make direct contact with experiments, which eventually represent the most important test for the validity of our theory.

Instead of trying to build a general model, we focus here on describing the case of protein adsorption on charged hydrogel-coated nanoparticles (which we sometimes refer to as nanogels). For this type of system, which still represent a broad category of important experimental cases, we show here how a simplified but robust model can be built by including a coarse-grained description of the major physical forces playing a role in the adsorption process, throwing out less relevant details and keeping all functional forms as simple as possible. For example, for the small but finite concentration of proteins found in these nanoparticles, the most relevant information about protein-protein interactions is well captured by a measurable thermodynamic quantity such as the second virial coefficient. Clearly, by using this parameter as a proxy for the full interaction potential we are making assumptions that restrict the validity of the model, which however remains general enough to be applicable to the majority of cases we would like to describe. In practice, we pay in generality what we get back in reliability and usability of the model. Based on similar premises, Yigit *et al* presented in Ref.¹⁴ a minimal thermodynamic model for protein adsorption onto charged nanoparticles that was shown to well compare with many available experimental data. For this reason, we decided to build our DDFT model by including the same terms. Hence, the free-energy functional we propose is the following:

$$\begin{aligned}
\mathcal{F} &= \mathcal{F}^{id} + \mathcal{F}^{ext} + \mathcal{F}^{exc} \\
&= \mathcal{F}^{id} + \left(\mathcal{F}^{ads} + \mathcal{F}^{electro} \right) + \mathcal{F}^{exc} \\
&= \mathcal{F}^{id} + \mathcal{F}^{ads} + \mathcal{F}^{Born} + \mathcal{F}^{Don} + \mathcal{F}^{exc} \\
&= \sum_p \int_V k_B T \rho_p(\mathbf{x}) \left[\ln \left(\frac{\rho_p(\mathbf{x})}{\rho_0} - 1 \right) \right] d\mathbf{x} \\
&+ \int_V \rho_p(\mathbf{x}) V^{ads}(\mathbf{x}) d\mathbf{x} - \int_V \rho_p(\mathbf{x}) V^{Born}(\mathbf{x}) d\mathbf{x} \\
&+ \int_V z_p \rho_p(\mathbf{x}) V^{Don}[\{\rho_p(\mathbf{x})\}^*] d\mathbf{x} \\
&+ \int_V \rho_p(\mathbf{x}) \mathcal{E}^{exc}(\{\rho_p(\mathbf{x})\}) d\mathbf{x}, \tag{8}
\end{aligned}$$

where the asterisk in the definition of V^{Don} means that when calculating its contribution to the chemical potential μ_p by taking the functional derivative, this should be done at a fixed value of V^{Don} to properly account for the charge-neutrality condition.

The first term in Eq. 8 \mathcal{F}^{id} is the ideal gas term. It accounts for the translational free-energy (entropy) of proteins in solutions. As previously explained, taken alone this term gives rise to the ideal diffusion equation. The remaining terms are instead due to interactions within the system. Two of them, \mathcal{F}^{ads} and $\mathcal{F}^{electro}$, depend on the protein-nanogel interaction,

whereas \mathcal{F}^{exc} accounts for protein-protein interactions.

\mathcal{F}^{ads} measures the intrinsic adsorption free-energy arising from protein-specific forces between proteins and the gel, such as hydrophobic and hydration forces or salt-bridges³⁴. We model this term as simply as possible using:

$$\mathcal{F}^{ads} = \int_V \rho_p(\mathbf{x}) V^{ads} d\mathbf{x} \tag{9}$$

$$V^{ads}(r) = S(r) \Delta G^{ads} \tag{10}$$

$$S(r) = [1 - \text{Fe}(r, R_{gel}, \sigma)]. \tag{11}$$

Here, ΔG^{ads} is the intrinsic adsorption energy per protein and S a switching function, describing the change of environment from that of the bulk gel to that of the bulk protein solution, where $\text{Fe}(r, \mu, \alpha) = 1/(1 + \exp[(r - \mu)/\alpha])$ is the Fermi function with inflection point at μ and width α , and $r = |\mathbf{x}|$ measures the distance from the centre of the nanoparticle. This choice of S ensures that the intrinsic interactions are local and present only when the protein effectively enters in the gel. A finite value for σ also implies that the gel-bulk solution boundary is not atomically sharp but varies within a distance σ of a few nanometers, comparable to the average cross-linking distance typically found in the polymer network of this system. For this reason, and to maintain consistency, the same type of spatial dependence is chosen also for the gel density and the protein's diffusion coefficient (which is a space dependent quantity varying between the bulk solution and the gel matrix), i.e.:

$$\rho_{gel}(r) = \rho_{gel}^{bulk} [1 - S(r)] \tag{12}$$

$$D_p(r) = D_p^{gel} + (D_p^{bulk} - D_p^{gel}) S(r) \tag{13}$$

where D_p^{bulk} and D_p^{gel} are the protein diffusion coefficient in the bulk solution and in the polymer gel, respectively^{35,36}, and ρ_{gel}^{bulk} is the polymer bulk number density. Other choices for these profiles with similar, physically justified shapes can be considered without affecting the simulation result.

The electrostatic free-energy $\mathcal{F}^{electro}$ is purely dictated by the charge of the protein and the nanogel, which in turn depend on the pH of the system as well as salt concentration and can be further split into two terms, \mathcal{F}^{Don} and \mathcal{F}^{Born} . \mathcal{F}^{Don} is an electrostatic contribution due to the difference in the electrostatic potential between the gel and bulk solution. This so-called Donnan potential, derived by imposing local charge neutrality in the system^{14,37}, depends on both the fixed charges of the nanogel as well as the mobile proteins and salt ions. The explicit form of the Donnan potential is:

$$e\beta V^{\text{Don}}(\mathbf{x}) = \tilde{V}^{\text{Don}}(\mathbf{x}) = \ln \left[\sqrt{y(\mathbf{x})^2 + 1} + y(\mathbf{x}) \right], \quad \text{with} \quad (14)$$

$$y(\mathbf{x}) = \frac{z_{\text{gel}}\rho_{\text{gel}}^c(\mathbf{x}) + \sum_p z_p \rho_p(\mathbf{x})}{z_s \rho_s^{\text{bulk}}} \quad (15)$$

where $\rho_{\text{gel}}^c(\mathbf{x})$ and z_{gel} are the number density of charged monomers (i.e. $\rho_{\text{gel}}^c = f_c \rho_{\text{gel}}$, where f_c is the fraction of charged monomers) and the monomer charge, respectively. Correspondingly, ρ_s^{bulk} and z_s are the bulk concentration of salt and the charge of a salt ion and finally z_p is the charge of a protein of type p .

In principle, one could calculate the full electrostatic energy of the system by building a density functional that includes also the densities of salt ions. However, the size of these ions is much smaller than that of a protein, hence they are a lot faster. This allows to assume that they are in local equilibrium with the density of the “slow” charges, those of the proteins and the gel. This separation of timescales greatly reduces the computational complexity of the problem⁸, and the electrostatic contributions can be efficiently calculated. One way to do this would be to fully solve the underlying Poisson-Boltzmann equations, at a fixed charge density given by the instantaneous realisation of the protein density field. However, if one coarse-grains the system on distances larger than the Debye screening length, a more efficient approach is to simply assume local charge neutrality, as we do here. With this choice, in the bulk of the gel we recover exactly the same value of the electric field obtained solving the Poisson-Boltzmann equation. Moreover, we recall that in our model all local properties including the electrostatic potential change from that of the gel to their bulk solution value within a distance of σ from the gel boundary (Eq. 11). Since our choice for σ is close to the Debye screening length ℓ_{Debye} (≈ 3.6 nm at the salt concentrations considered here), our minimal model is also in semi-quantitative agreement with the Poisson-Boltzmann solution for the *variation* of the electrostatic field at the gel-bulk solution interface.

The second term in the electrostatic energy is the Born transfer energy F^{Born} , which simply describes the change in the self-energy of the charged proteins due to the different screening properties in the gel matrix and the bulk solution, whose known form is³⁴:

$$\beta V^{\text{Born}}(\mathbf{x}) = \frac{z_p^2 l_B}{2r_p} \frac{\kappa(\mathbf{x}) r_p}{(1 + \kappa(\mathbf{x}) r_p)} \quad (16)$$

$$\kappa(\mathbf{x}) = \sqrt{4\pi\lambda_B \rho_{\text{local}}(\mathbf{x})} \quad (17)$$

$$= \sqrt{4\pi\lambda_B (\rho_{\text{gel}}^c(\mathbf{x}) + \rho_s(\mathbf{x}))}$$

$$\rho_s(\mathbf{x}) = \rho_s^{\text{bulk}} \left(e^{(-z_s \tilde{V}^{\text{Don}}(\mathbf{x}))} + e^{(+z_s \tilde{V}^{\text{Don}}(\mathbf{x}))} \right) \quad (18)$$

where $\lambda_B = \frac{e^2}{4\pi\epsilon_0\epsilon k_B T}$ is the Bjerrum length (taken to be 0.7 nm in water at room temperature) and $\kappa(\mathbf{x})$ is the position-dependent screening length which depends on the total ionic concentration of the gel and salt ions, ρ_{local} . For a cross-linked nanogel network, where the monomer density is constant in space, ρ_{gel}^c is given by Eq. 12 multiplied by the fraction of charged monomers f_c , whereas the salt charge density instead is again dictated by local charge neutrality, consistently with our previous choice of the Donnan potential to describe the electrostatic energy in the system.

Finally, the fourth term in the expansion of the free-energy functional depends on the excess free-energy density per particle ϵ^{exc} , and measures the strength of protein-protein excluded-volume interactions¹⁴. In principle, the excess free-energy can be significant at moderate packing fractions and becomes very high close to the crystallisation density of hard-spheres. However, these are well below the experimental packing fraction typically achieved in protein adsorption, at which ϵ^{exc} is a relatively minor perturbation to the total free-energy with respect to all other terms present in the system (see for example Fig. 2). For this reason, we only consider its value in the second order expansion in density, the so-called B_2 approximation. Not only this further simplifies our calculations, but B_2 is also an experimentally measurable quantity which can be easily accessed from the osmotic pressure as a function of density for a protein solution. Explicitly, this choice for ϵ^{exc} results in the following formula:

$$\begin{aligned} \mathcal{F}^{\text{exc}} &= \sum_p \int_V \epsilon(\{\rho_p(\mathbf{x})\}) \rho_p(\mathbf{x}) d\mathbf{x} \\ &= -\frac{1}{2} k_B T \sum_{i,j} B_2^{ij} \int_V \rho_i(\mathbf{x}) \rho_j(\mathbf{x}) d\mathbf{x}, \end{aligned} \quad (19)$$

where the indices i and j run over all protein types in the system. It was shown in¹⁴ that a reasonable value to take for B_2 is that for hard-spheres of the same mean size as the globular protein, given by:

$$B_2^{ij} = \frac{2\pi}{3} \left(\frac{\sigma_i + \sigma_j}{2} \right)^3 \quad (20)$$

where σ_i (σ_j) is the effective hard-core diameter of protein i (j). In principle, to account for polymer-protein excluded volume interactions, the sum in Eq. 19 should include one term depending on the polymer density ρ_{poly} . The latter could also be considered another dynamic variable of the system, and its spatially dependent field treated at the same level as that of the protein, as done for example in⁸. Since for charged gels the polymer network is relatively rigid and the cross-linking distance is much larger than the protein size, we treat instead the polymer as a fixed effective excluded volume zone, and thus scale all protein densities ρ_i in Eq. 19 in the following way:

$$\rho_i(\mathbf{x}) \rightarrow \xi(\mathbf{x}) \rho_i(\mathbf{x}) = \left(\frac{1}{1 - \rho_{poly}(\mathbf{x}) v_{mon}} \right) \rho_i(\mathbf{x}), \quad (21)$$

where v_{mon} is the effective volume occupied by a monomer, which for our system is approximately 0.3 nm^3 ¹⁴. Outside of the gel, $\xi = 1$ and no scaling occurs, whereas inside the bulk polymer an increase in the number density of about 8% is observed.

Finally, combining the previous definitions for the various terms appearing in Eq. 8 with Eq. 5, we obtain for the chemical potential of the specie p as a function of $\rho_p(\mathbf{x}, t)$:

$$\begin{aligned} \beta \mu_p(\mathbf{x}, t) = & \ln \left(\frac{\rho_p(\mathbf{x}, t)}{\rho_0} \right) + \beta \Delta G^{ads} S(|\mathbf{x}|) \\ & + \beta V^{\text{Don}}(\mathbf{x}, t) + \beta V^{\text{Born}}(\mathbf{x}, t) - \sum_j B_2^{pj} \rho_j(\mathbf{x}, t). \end{aligned} \quad (22)$$

By plugging Eq. 22 into the generalised diffusion equation, Eq. 3, we fully define the dynamics of our system, which we will investigate later in Sec. 4.

3 Diffusion timescales from simple analytical models

Before turning to fully solve the complex numerical equations described in the previous session, it is instructive to have at least a rough idea of the timescales involved in this problem by looking at a couple of analytically solvable models.

3.1 Free diffusion in an open, spherically symmetric environment (Debye result)

When modelling adsorption phenomena, many authors resort to the famous Debye formula, which solves the problem of finding the steady-state profile of a diffusing, non interacting specie around a spherically absorbing sink in contact with an

infinite reservoir at density ρ_p^{bulk} . In practice, this requires solving the following equation for the radial density of the specie $\rho_p(r)$:

$$\begin{cases} \frac{1}{r^2} \frac{\partial}{\partial r} r^2 D_p \frac{\partial \rho_p(r)}{\partial r} = 0 \\ \rho_p(r) |_{r=R_{gel}} = 0 \\ \rho_p(r) |_{r=\infty} = \rho_p^{bulk} \end{cases} \quad (23)$$

whose solution, assuming D_p is constant in space, reads

$$\rho(r) = \rho_p^{bulk} \left(1 - \frac{R_{gel}}{r} \right). \quad (24)$$

Given that this is a problem of simple diffusion with no terms apart the ideal one, the flux is equal to $J = -D_p \frac{\partial \rho}{\partial x}$, from which follows the famous Debye formula for the steady-state flux:

$$\begin{aligned} k_{debye} &= 4\pi r^2 J(R_{gel}) \\ &= 4\pi r^2 D_p \frac{\partial \rho}{\partial r} |_{r=R_{gel}} \\ &= 4\pi R_{gel} D_p \rho_p^{bulk} \end{aligned} \quad (25)$$

It should be emphasised that Eqs. 23 and 25 describe adsorption by a perfectly adsorbing sink, whereby a particle, once it reaches the sink, disappears from the solution. Given that particles never accumulate at the boundary of the sink, and the bulk provide an infinite amount to replace those that are adsorbed, the flux is never zero and indeed these equations describe a non-equilibrium steady state problem.

Whereas this formula can then approximate the flux for intermediate times (after a fast transient time $t_{relax} = R_{gel}^2 / 2D_p \approx 0.1 \text{ ms}$ for our system), in the real scenarios particles will accumulate at a boundary, generating a counter-gradient that will in fact slow down and eventually stop diffusion. Hence care should be taken when estimating protein loading speed using Eq. 25. However, we note here that whereas mass conservation will slow down diffusion, other fluxes present in the system not accounted in this simple description *might* accelerate it, balancing the effect. Here we want to estimate the loading timescale for a specific case study: the adsorption of positively charged Lysozyme onto negatively charged PNIPAM nanogels. In this system, both electrostatic interaction and the intrinsic adsorption energy speed up protein adsorption compared to ideal diffusion. Hence, in this particular case we expect a partial cancellation of errors to improve our estimate.

Given these premises, we will calculate as a measure of the speed of the loading kinetics the time taken by the nanoparticle to reach half the equilibrium loading, i.e. $t_{1/2}$. To do this,

however, we clearly require one important additional information, i.e. the total number of adsorbed particles at equilibrium. From experimental measurements¹⁴, we know that about $5 - 7 \cdot 10^4$ proteins are adsorbed on the nanogel. Since the number of adsorbed proteins per unit time (within this Debye approximation) is simply given by $N(t) = k_{Debye}t = 4\pi R D_p \rho_p^{bulk} t$ we obtain by inverting this equation and setting $N = 6 \cdot 10^4$, $D_p = 0.1 \text{ nm}^2/\text{ns}$, $R = 150 \text{ nm}$ and $\rho_p^{bulk} = 2 \cdot 10^{-4} \text{ Mol}$ a value of $t_{1/2} \approx 1 \text{ ms}$. As we will see, for an effect of cancellation of errors previously discussed, this estimate will not be too far from the results obtained solving the much more complex DDFT equations.

3.2 Free diffusion in a closed, spherically symmetric environment

To account at least for mass-conservation effects within the bulk solution, we should solve the ideal diffusion equation under more realistic boundary conditions than those implied in the Debye treatment. Hence, we solve the diffusion equation for a closed, spherically symmetric environment.

We thus have, in spherical coordinates:

$$\left\{ \begin{array}{l} \frac{\partial \rho_p(r,t)}{\partial r} = \frac{1}{r^2} \frac{\partial}{\partial r} r^2 \frac{D_p \partial \rho_p(r,t)}{\partial r} \\ \frac{\partial \rho_p(r,t)}{\partial r} \Big|_{r=R_{core}} = 0 \\ \frac{\partial \rho_p(r,t)}{\partial r} \Big|_{r=L} = 0 \\ \rho_p(r,t) \Big|_{t=0} = \rho_p^{bulk} \theta[r - R_{gel}] \end{array} \right. \quad (26)$$

where R_{core} is the radius of the nano particle hard-core (see Fig. 1), and the outer boundary L depends on the nanogel number density ρ_{np} , as specified later in Sec. 4. The initial density profile is taken to be a homogeneous density equal to the initial bulk density value ρ_p^{bulk} , except in the nanogel where it is taken to be zero, corresponding to a possible setup where nanoparticles are inserted in an otherwise equilibrated solution of proteins. This problem can be fully solved analytically by standard Fourier techniques. We will only report here the final form of the solution for clarity, where we also assumed D_p to be constant in space

$$\rho_p(r,t) = C_0 + \frac{1}{r} \sum_{n=1}^{n=\infty} \exp(-\lambda_n^2 D_p t) N_n^{-1} C_n \phi_n(r) \quad (27)$$

$$N_{\lambda_n}^{-1} = \quad (28)$$

$$\frac{2}{\left[\left(\lambda_n^2 + \frac{1}{R_{core}^2} \right) \left((L - R_{core}) - \frac{1}{L \left(\lambda_n^2 + \frac{1}{L^2} \right)} \right) \right] + \frac{1}{R_{core}}} \quad (29)$$

$$C_n = \int_{R_C}^L r' \theta(r' - R_{gel}) \phi_n(r') dr' \quad (29)$$

$$\phi_n(x) = \lambda_n \cos(\lambda_n r) + \frac{1}{R_{core}} \sin(\lambda_n r) \quad (30)$$

where C_0 is nothing but the average value of the initial density in the domain, i.e.

$$C_0 = \frac{3}{4\pi(L^3 - R_{core}^3)} \int_{R_{core}}^L 4\pi r^2 \rho_p^{bulk} \theta(r - R_{gel}) dr, \quad (31)$$

and λ_n is given by the solution of the following transcendental equation

$$\tan(\lambda_n(L - R_{core})) = \frac{\lambda_n(L - R_{core})}{1 + \lambda_n^2 L R_{core}}, \quad (32)$$

where n labels the infinitely many solution for this equation. The solution to this problem is quite instructive, and we discuss some of its main features here. First of all, a timescale $\tau_D = \frac{(L - R_{core})^2}{D_p}$ appears. Note that this timescale does not contain any reference to R_{Gel} , i.e. the radius of the nanogel. Moreover, at the typical densities encountered in experiments, one has that $L \gg R_{core}$, hence the only relevant timescale is controlled by the nanogel average distance L , itself a function of the nanogel density, $L \approx \rho_{np}^{-1/3}$ (see Sec. 4). This would mean that the adsorption kinetics for micron- or nano-sized gels, if measured at the same number density, will be the same within this model. If experiments instead are made at constant packing fraction $\rho V_{nanogel}$, which scales as R_{gel}^3 , then the loading dynamics will be many orders of magnitude faster for nanogels. This can partially rationalise the very different timescales observed in the experiments for these two systems^{5,38}. If we plug into the definition of τ_D the values of L for the experiments we are trying to describe¹⁴ (see Sec. 4), which is about 10^3 nm , and the diffusion coefficient of lysozyme in water, which is of order $D_p \approx 0.1 \text{ nm}^2/\text{ns}$ ⁵, by truncating Eq. 30 to the first few terms in n , we obtain an estimate of $t_{1/2} \approx 2 \cdot 10^{-3} \tau_D = 2 \cdot 10^{-2} \text{ ms}$.

The reason for which diffusion is here much faster than for the Debye case is that we properly took into account the full

density evolution, which has initially a strong density gradient -hence associated flux- at the nanogel/solution boundary, whereas in the Debye case we simply used the steady state value of the flux to calculate the loading. Regardless, we will see later in Sec. 4 how neither the timescales nor the density profile obtained from the solution of the ideal diffusion equation correspond to what is observed for our DDFT model, warranting that ideal diffusion equations should be taken very carefully when used as an interpretative model for experimental data, even from a qualitative point of view.

4 Numerical results from the DDFT equations

In this section we will present a series of results from the full numerical solution of the DDFT equation. The associated PDE for the time-evolution of the density field was solved by discretising the problem on a fixed grid of spacing 0.5 nm and propagating the equation of motion using a 4th order Runge-Kutta method with a timestep in the range [0.025 – 0.05] ns depending on the parameters. Simulations were run for a number of timesteps in the range [10⁷ – 10⁹], and for all of them mass was conserved within less than a 1% error.

The boundary conditions to solve Eq. 3 are dictated by our system. One of the boundaries is the nanoparticle hard-core on which the polymeric gel is grafted. For all intense and purposes, this core can be safely regarded as a barrier that proteins cannot penetrate. A no-flux boundary condition at $r = R_{gel}$ takes care of that. The second boundary is given by the experimental setup we want to describe. In a real experiment, nanoparticles are found in solution at a low but finite density, and in principle their exact position will matter for the protein adsorption dynamics: the full problem would couple the position of all nanoparticles to the protein density field. Instead of solving this very complex computational problem, we take a statistical approach and use instead a cell-model¹⁴. Each nanoparticle is supposed to be isolated in a spherical cell of fixed volume and the sum of all volumes must fill the whole space, giving the following condition for the cell radius R_{cell} :

$$\begin{aligned} N_{np}V_{cell} &= V_{tot} \\ \rightarrow R_{cell} &= \left(\frac{3V_{tot}}{4\pi N}\right)^{1/3} = \left(\frac{3}{4\pi\rho_{np}}\right)^{1/3} \end{aligned} \quad (33)$$

where N_{np} is the number of nanoparticles present in solution and ρ_{np} their number density. This is a valid assumption when nanogels do not tend to aggregate but remain dispersed. In this model, a no-flux boundary condition naturally arises at $r = R_{cell}$, because the radial flux from neighbouring cells exactly compensates.

To allow for the tightest possible comparison to experiments, we will analyse the same system as in Ref.¹⁴. Briefly, a nanogel with a hard-core radius of $R_{core} \approx 60$ nm with a charged polymer corona of 90 nm, hence $R_{gel} \approx 150$ nm. There are approximately $3.7 \cdot 10^6$ monomers for each nanogel, about which $4.9 \cdot 10^5$ carry a net charge of $-1e$ (i.e. $f_c \approx 13\%$), for a total charge density of $\rho_{gel}^c \approx 4 \cdot 10^{-2} e/\text{nm}^3$. For comparison, the average concentration of cations (anions) due to the dissociated salt is almost an order of magnitude smaller, i.e. $\rho_s = 7$ mMol, or $\approx 4 \cdot 10^{-3} e/\text{nm}^3$. The volume of each monomer is estimated to be about 0.3 nm^3 so that the total excluded volume in the gel is $\approx 8\%$. The number concentration of nanogels is $\rho_{np} = 8.42 \cdot 10^{-10} \text{ M}$, i.e. about $1/\mu\text{m}^3$. This concentration is related to the average distance between gel particles by Eq. 33, which gives $R_{cell} \approx 780$ nm, about 5 times the radius of the gel itself. When not specified otherwise, the protein under investigation is Lysozyme, which carries a net charge of $+7e$ at the pH=7.2 considered. The initial bulk number density of protein is taken to be $\approx 5 \cdot 10^4 \rho_{np}$, corresponding to $5 \cdot 10^{-5} / \text{nm}^3$. The diffusion constant of Lysozyme in water is taken to be $10^{-1} \text{ nm}^2/\text{ns}$, in accordance with both experimental and theoretical values in the literature^{39,40}, whereas that in the gel it is taken to be an order of magnitude slower, a reduction consistent to that observed in other similar polymeric systems⁵. The only additional necessary parameter to model the kinetics is the intrinsic adsorption energy ΔG^{ads} of the protein, which can be extracted from experiments probing the thermodynamics of protein adsorption for the same system¹⁴. For Lysozyme, this was determined to be equal to $7.25k_B T$.

Before we proceed to discuss the results of our numerical modelling, we should point out that in order to simplify the problem our model does not take into account the fact that the polymer gel can shrink upon protein adsorption. Experimentally, for the initial bulk protein concentration studied in this case, the maximum reduction in the polymer radius, achieved at equilibrium, is roughly 10%¹⁴. Since the polymer volume, and hence the number of protein's adsorption sites (in the sense specified in Ref.¹⁴), turns out to be an important quantity to get a realistic estimate of the loading kinetics, we take as the fixed value for the radius of the gel the equilibrium value. Whereas this simplification might change the exact numerical results, it does not impact in a significative way our estimates for the orders of magnitude nor the trends observed.

4.1 Equilibrium

Before discussing the dynamics of our system, it is of interest to look at the final equilibrium solution, in order to highlight the role played by the various term in determining the final equilibrium density profile $\rho_p^e(\mathbf{x})$. This can be obtained by looking for the density profile for which $J(\mathbf{x}) = 0$, or, equiva-

lently, minimising the free-energy functional (Eq. 6) under the constraint of a fixed number of proteins, leading to:

$$\rho_p^e(\mathbf{x}) = \rho_0 e^{(-\beta\mu_p^{eg})} e^{\left[-\beta\left(V^{ext}(\mathbf{x}) + \epsilon^{exc}(\{\rho_p^e(\mathbf{x})\}) + \rho_p^e(\mathbf{x}) \frac{\partial \epsilon^{exc}(\{\rho_p^e(\mathbf{x})\})}{\partial \rho_p}\right)\right]} \quad (34)$$

where the quantity $\rho_0 e^{(-\beta\mu_p^{eg})}$ is determined by imposing a fixed number of proteins N_p in our cell volume for each species in the system, i.e.

$$\int_{R_{core}}^{R_{cell}} 4\pi r^2 \rho_p^e(r) dr = N_p = V_{cell} \rho_p^{bulk}. \quad (35)$$

where ρ_p^{bulk} is the *initial* bulk concentration of protein p (note that due to mass conservation, the density of proteins in the bulk will diminish due to adsorption onto the nanoparticle). In general, when inter-particle interactions are present and hence the density appears in both sides of Eq. 34, a closed formula for ρ_p^e cannot be found, and the problem must be solved iteratively starting with a trial density and iterating until self-consistency is achieved.

We report in Fig. 2 the value of the various terms in Eq 8 for the initial (top) and equilibrium (bottom) density distribution.

An important feature to notice in these profiles is the change of some of the thermodynamic forces in their slope at the gel/bulk solution boundary (i.e. $R=1$), since this is related to the adsorption flux through the equation

$$J_p^i(t) = -D_p(R_{gel}) \rho_p(R_{gel}, t) \frac{\partial \beta \mu_p^i(R_{gel}, t)}{\partial r} \quad (36)$$

where the superscript i labels the specific thermodynamic potential considered (e.g V^{Don} , V^{Bom} , ...). Indeed, this change means that whereas initially all thermodynamic forces drive the system towards absorbing protein, closer to equilibrium only the Born and intrinsic energy term favour adsorption, whereas the ideal and excess terms, as well as the Donnan potential, prevent it. It is the balance between these opposing terms that determines the final equilibrium, and strongly influences the observed dynamics of the system.

4.2 Dynamical behaviour

We report the full time evolution of the density profile for the system in Fig. 3. Let us first discuss these profile qualitatively. Three distinct regimes can be observed. At very short timescales ($t < 10\mu s$), a density instability is generated at the boundary between the gel and bulk surface, which propagates towards the nanoparticle hard core. This density peak

stems from competition between a very strong energy gradient at the gel-bulk boundary which pushes protein towards the gel together with the reduced diffusion coefficient in the gel region, which is about 1/10 that in the bulk solution, which causes proteins to accumulate at the interface. At intermediate timescales ($t < 110\mu s$), the density peak diffuses far enough towards the gel/hardcore boundary, an appreciable concentration of protein builds up in this region, and the density peak becomes more diffuse, eventually reaching a width approximately equal to the gel width. At this point, a step-like density profile is obtained, and at later times the only qualitative change in the density profile is its height, which grows in time until the full equilibrium loading is reached.

A question that naturally arises is whether a similar dynamical behaviour can be reproduced using a simple diffusion model where only the ideal term is retained, but we still account for the space-dependence of the diffusion coefficient to make a fair comparison. This is what many kinetic models of protein adsorption assume either implicitly or explicitly, completely neglecting the role of energy gradients in the system⁵. Fig. 4 reports for comparison the evolution of the density profile for the same type of protein described in Fig. 3 but described in terms of the ideal diffusion equation, where the diffusion coefficient has been taken to have the same spatial dependency as for the DDFT model to allow for proper comparison:

It is evident that the dynamics is not only just quantitatively approximate but also qualitatively very different compared to the one obtained using a more realistic model. Moreover, the timescales are clearly off by more than an order of magnitude, given that the density profile for purely ideal diffusion has almost reached its equilibrium value in half a millisecond, in contrary to the full description where at five milliseconds the density profile is still relatively far from being equilibrated. In principle, one could argue that DDFT models might not reproduce the loading dynamics better than the ideal diffusion equation. To show this is not the case, we report for both models in Fig. 5 the time dependence of the loading $\Theta(t) = N(t)/N(\infty)$ (where $N(t)$ is the number of adsorbed proteins, obtained by simply integrating the density over the whole gel volume) and compare it to that extrapolated from fitting of experimental data, as shown in Ref.³⁸. In this latter paper, it was shown that an empirical Langmuir fit was able to reproduce, using the same parameters, data at different densities. In order to compare our data with those from experiments, we scaled the experimental value to the same protein density studied here*.

It should be clear from Fig. 5 that our DDFT description, although still not in complete quantitative agreement with experimental data, is a much better representation than an ideal

* simulations of the density for which experimental data is directly available is not possible since this would require simulating timescales a couple of orders of magnitude higher than those accessible within our model, due to computational limitations

diffusion model, where the dynamics is off by more than one order of magnitude.

Since an important fact is that ideal diffusion completely neglects the important fluxes due to energy gradient in the systems, it is illuminating to look at how much these contribute to protein loading, as shown in Fig. 6, where we plot the ideal and excess protein flux at the gel-solution boundary (the sum of which, by integration over time, gives the loading). As observed in Fig. 6, the ideal flux in both models are similar. However, the real flux is the sum of the ideal *and* excess flux, the latter being zero in an ideal diffusion model. In this regard, we notice how the excess flux is always at least comparable if not dominant w.r.t the ideal one, with the result that not taking it into account leads to a wrong estimate of the loading.

In our model, the excess flux is always positive, hence it leads to a higher number of adsorbed proteins per unit time in the DDFT scenario. This is not in contrast with ideal diffusion models relaxing to equilibrium much faster than the more realistic DDFT description because the equilibrium number of proteins calculated within an ideal model is orders of magnitudes smaller than that from DFT. In fact, underestimation of the equilibrium amount of protein is possibly the largest source of error in using the ideal diffusion equation to model protein adsorption⁵, since it can only predict a final flat equilibrium profile where the density is constant throughout the system. However, as expected from simple thermodynamics arguments, a non-homogeneous density must appear whenever any type of gel/protein interaction is present. Hence, care should be taken when using ideal diffusion models to analyse experimental data. For example, in Ref.⁵ Li *et al.* found that in order to obtain the correct timescales, they had to assume the presence of trapping binding sites that reduce the mobility of the proteins, effectively inducing a diffusion constant about 2 to 3 orders of magnitudes lower than that expected for similar polymer/protein systems. Such a small value is probably an artefact arising from not including any electrostatic driving force in their description, since in our DDFT model we were able to obtain the correct timescale without assuming such a surprisingly small diffusion coefficient. The importance of electrostatics is pointed out by the fact that, in the same experiments, they found that the number of expected binding sites (which determines the effective diffusion coefficient) is strongly dependent on pH, varying by a factor of 20 in the pH range [3 – 7]⁵.

4.3 Parametric study

Given that we observe both qualitative and semi-quantitative agreement with experiments, we can confidently use the current model to investigate the sorption kinetics for different sce-

	$t_{1/2}$ (μs)	Trend
Z		
0	90	non-monotonous
1	260	
2	510	
3	620	
5	560	
$\rho_p^{bulk} / \rho_p^{ref}$		
1/8	340	decreasing
1/4	330	
1/2	300	
1	270	
2	210	
$\rho_{np} / \rho_{np}^{ref}$		
1/8	370	decreasing
1/4	350	
1/2	320	
1	270	
2	200	
$ \beta\Delta G^{ads} $		
0	160	increasing
1	270	
2	390	
3	530	

Table 1 Time to reach half the equilibrium loading $t_{1/2}$ for the various parameters combinations investigated in our system. Note in particular that $t_{1/2}$ as a function of valence shows a peculiar non-monotonous behaviour, possibly due to a maximum in the total amount of proteins adsorbed at equilibrium as a function of valence. ρ_p^{ref} and ρ_{np}^{ref} are equal to $2.02 \cdot 10^{-4}$ M and $3.37 \cdot 10^{-9}$ M, respectively.

narios, and try to rationalise the observed trends. In particular, we assess here how the dynamics changes as a function of four important parameters characterising our system, i.e. protein valence, nanoparticles and protein's concentration and intrinsic adsorption energy. We do this by looking at both the unnormalised and normalised amount of adsorbed proteins, $N(t)$ and $\Theta(t)$. As previously done in Sec. 3 we will take as an informative quantity to measure the speed of the kinetics the time to achieve half the equilibrium loading, $t_{1/2}$, which we report in Table 1. The standard values for the parameters in the following simulations are $\beta\Delta G^{ads} = -1$, $\rho_p = 2.02 \cdot 10^{-4}$ M, $\rho_{np} = 3.36 \cdot 10^{-9}$ M and $Z = 1$, and in each set of simulations one of this quantity is varied keeping the other fixed. The parameters describing the nanoparticle, such as its radius or that of the polymer gel coating it, are the same as those for the Lysozyme model. Fig. 7,8 and Table 1 summarise our results:

The observed trends in Fig. 7 and Fig. 8 can be rationalised in terms of two balancing mechanisms. On the one side,

higher driving forces, for example a lower ΔG^{ads} or higher protein concentration should lead to a faster kinetics, given that higher fluxes are expected. The same should happen for lower nanoparticle concentrations, for which the counter flux, introduced via the boundary conditions that account for proteins being adsorbed by neighbouring particles, is reduced. This is indeed the case, because at any one time the amount of adsorbed proteins is an increasing function of these driving forces, as can be observed from the unnormalised adsorption profiles of Fig. 8. On the other side, however, higher driving forces (with the only exception of the protein's valence, which deserve a separate discussion later) also lead to a higher number of adsorbed proteins at equilibrium.

Clearly, if both the equilibrium number of proteins adsorbed and the average fluxes were linearly increasing functions of these driving forces, $\Theta(t)$ for different parameter values, i.e. Fig. 7 should collapse onto a single curve. Instead, a very different behaviour is observed. In fact, it turns out that the increase in the total flux when higher driving forces are present is not always enough to compensate for the higher value of proteins that must be adsorbed to reach equilibrium, hence the loading dynamics can be slower. For example, loading as a function of increasing (in modulus) adsorption energy becomes slower, whereas it is faster if we simply increase the initial bulk concentration of proteins, ρ_p^{bulk} , despite in both ways we are increasing both the adsorption fluxes and $N(\infty)$. However, although $N(\infty)$ as a function of ρ_p^{bulk} grows more rapidly than for ΔG^{ads} , its associated flux increases even faster and the overall loading dynamics is actually faster and not slower for this latter case. As this example shows, the fact that both fluxes and equilibrium adsorption are highly non-linear functions of the control parameters implies that predictions based on simple arguments can be highly misleading, and one really has to solve the full equation of motion to rationalise these behaviours. To make an even simpler example, let us just point out that for ideal diffusion the loading dynamics is not even a function of the bulk protein concentration, ρ_p^{bulk} .

An even stronger manifestation of non-linear behaviour can be observed in our system for the case of $\Theta(t)$ as a function of protein's charge Z . In this case, $t_{1/2}$ has a maximum for $Z = 3$ and then decreases, a type of non-monotonic behaviour which would be difficult to predict without a full DDFT modelling. This maximum again arises since the total amount of adsorbed proteins at equilibrium $N(\infty)$ as a function of their charge rapidly saturates (see Fig. 8 and compare the $Z = 3$ and $Z = 5$), whereas the thermodynamic force for adsorption does not (at least until charge inversion of the loaded gel occurs). Saturation is expected because of two competing effects. On the one hand, when a protein of unlike charge absorbs the system decreases its energy by an amount $|ZV^{Don}|$. However, V^{Don} is itself a function of the adsorbed charge, and becomes lower the higher the number of proteins in the gel. Hence,

a maximum amount of adsorbed particles exists, when the adsorption of one more protein would effectively increase the total electrostatic potential felt in such a way that no-more energy is gained. Given the form of V^{Don} (Eq. 15), this is expected to happen earlier for proteins of higher charge.

We would like to stress the fact that it would be difficult to rationalise these effect looking purely at the loading dynamics $\Theta(t)$ and not at the "raw" quantity $N(t)$, since the latter typically shows a different behaviour. In particular, terms as "fast" or "slow" dynamics should be used based on one or the other quantity in order to avoid confusion, especially when comparing different systems, like for example nanoparticles of different size. In this regard, we notice that many analysis of experimental results are often based on $\Theta(t)$ alone, although in principle such techniques have access to the raw quantity as well.

What additional insights do these simulations offer regarding protein adsorption on nanogels? One thing to notice is that the parameters' range scanned in this systematic study covers typical values observed for protein-nanogels system, and the timescales observed should thus be indicative of those expected in realistic scenarios. In this regard, we would like to highlight the fact that here protein adsorption occurs on timescales of a few milliseconds. Whereas this will depend on the exact concentration of both nanoparticles and proteins, it is nonetheless many orders of magnitude faster than that observed in typical anti-fouling applications such as PEG-coated surfaces⁴, or for bare nanoparticles^{6,7}. Hence, it is reasonable to assume that in this system the protein's corona always reaches equilibrium with the local environment. This fact can have important repercussions on large-scale models for pharmacokinetics, since it would justify modelling the nanoparticles behaviour in the human body assuming the protein corona (i.e. the nanoparticles "biological identity"^{3,41}) rapidly adapts to the changes in pH, protein and salt concentration found in different tissues (given that transport between different parts of the body of these nanoparticles by either diffusion or convection through the blood-stream occurs on timescales a few orders of magnitude higher). This is clearly not the same behaviour one can assume to describe, for example, protein induced degradation in a biomedical implant, since the protein adsorption kinetics in this case will necessarily play a much more important role given the long times required to achieve equilibrium.

These conclusions might be challenged when considering the case of competitive protein adsorption when multiple types are present, which will be studied in a future publication.

5 Conclusions

In this paper, we presented a theoretical model based on DDFT to describe protein adsorption on charged, polymer-coated nanoparticles. Compared to simpler descriptions of the kinetics such as models based on ideal diffusion or Langmuir-type kinetics, DDFT offers a natural and very general framework to include in a controlled manner the effect of all possible interactions within the system, and to separately study their effect. Here, we concentrated on including those effects which proved to be useful to rationalise the adsorption thermodynamics in the system, and separate interactions into non-specific, global electrostatic interactions as captured by the concept of the Donnan potential and Born energy, and protein-specific, intrinsic effect such as those arising from hydrophobic interactions and excluded volume effects¹⁴.

The model is constructed so that once the intrinsic adsorption energy is obtained by fitting calorimetric curves probing the thermodynamics of protein adsorption in the system, the kinetics can be described with no additional parameter. Using such a procedure, we are able to reproduce on a semi-quantitative level the observed experimental loading kinetics of Lysozyme on PNIPAM coated nanogels.

Finally, we presented a parametric exploration of the model, where we studied the variation in the loading kinetics for various quantities of interest, such as protein's valence and intrinsic adsorption energy, as well as their concentration and that of the nanogels in solution. Curiously, in all cases the timescale for protein adsorption is on the millisecond scale, suggesting fast equilibration of the protein corona with the local environment for typical settings where nanoparticles are used, for example, for drug delivery.

Before we conclude, we have a last remark. Although we applied it here for the case of a single-component system to present its main feature, the model can be easily extended to the case of multi-component systems, where possible cooperative and/or competitive adsorption effects are expected, giving rise to a peculiar, non-monotonic dynamics in the adsorption profiles such as those observed in the so-called "Vroman effect"^{42,43}. Modelling of such phenomena are currently under investigation, and will be presented in future publications.

6 Acknowledgements

S.A-U and J.D acknowledge funding from the Alexander von Humboldt (AvH) Foundation via a Post-Doctoral Research Fellowship. All authors acknowledge support from the Helmholtz Virtual Institute (HVI) "Multifunctional Materials in Medicine" (Berlin and Teltow), Germany.

References

- 1 K. Nakanishi, T. Sakiyama and K. Imamura, *Journal of Bioscience and Bioengineering*, 2001, **91**, 233–244.
- 2 S. D. D. Tenzer, J. Kuharev, A. Musyanovych, V. Fetz, R. Hecht, F. Schlenk, D. Fischer, K. Kiouptsi, C. Reinhardt, K. Landfester, H. Schild, M. Maskos, S. K. Knauer and R. H. Stauber, *Nature Nanotechnology*, 2013, **8**, 772–781.
- 3 M. Monopoli, A. Christoffer, A. Salvati and K. Dawson, *Nature Nanotechnology*, 2012, **7**, 779–786.
- 4 Q. Wei, T. Becherer, S. Angioletti-Uberti, J. Dzubiella, C. Wischke, A. Neffe, A. Lendlein, M. Ballauff and R. Haag, *Angewandte Chemie International Edition*, 2014.
- 5 Y. Li, Z. Zhang, H. P. van Leeuwen, M. A. Cohen Stuart, W. Norde and J. M. Kleijn, *Soft Matter*, 2011, **7**, 10377–10385.
- 6 D. Dell'Orco, M. Lundqvist, C. Oslakovic, T. Cedervall and S. Linse, *PLoS ONE*, 2010, **5**, e10949.
- 7 F. Darabi Sahneh, C. Scoglio and J. Riviere, *PLoS ONE*, 2013, **8**, e64690.
- 8 F. Fang and I. Szleifer, *Biophysical Journal*, 2001, **80**, 2568 – 2589.
- 9 F. Fang and I. Szleifer, *The Journal of Chemical Physics*, 2003, **119**, 1053–1065.
- 10 M. A. Carignano and I. Szleifer, *Colloids and Surfaces B: Biointerfaces*, 2000, **18**, 169 – 182.
- 11 F. Fang, J. Satulovsky and I. Szleifer, *Biophysical Journal*, 2005, **89**, 1516 – 1533.
- 12 J. B. Schwartz, A. P. Simonelli and W. I. Higuchi, *Journal of Pharmaceutical Sciences*, 1968, **57**, 274–277.
- 13 Y. Samuelov, M. Donbrow and M. Friedman, *Journal of Pharmaceutical Sciences*, 1979, **68**, 325–329.
- 14 C. Yigit, N. Welsch, M. Ballauff and J. Dzubiella, *Langmuir*, 2012, **28**, 14373–14385.
- 15 U. M. B. Marconi and P. Tarazona, *The Journal of Chemical Physics*, 1999, **110**, 8032–8044.
- 16 M. Rex and H. Löwen, *Phys. Rev. Lett.*, 2008, **101**, 148302.
- 17 M. Rex, H. H. Wensink and H. Löwen, *Phys. Rev. E*, 2007, **76**, 021403.
- 18 R. Wittkowski and H. Löwen, *Molecular Physics*, 2011, **109**, 2935–2943.
- 19 B. D. Goddard, A. Nold, N. Savva, P. Yatsyshin and S. Kalliadasis, *Journal of Physics: Condensed Matter*, 2013, **25**, 035101.
- 20 J. Wu and Z. Li, *Annual Review of Physical Chemistry*, 2007, **58**, 85–112.
- 21 R. Evans, *Advances in Physics*, 1979, **28**, 143–200.
- 22 J. P. Hansen and I. MacDonald, *Theory of Simple Liquids*,

-
- Academic Press, 4th edn., 2013.
- 23 M. Schmidt and J. M. Brader, *The Journal of Chemical Physics*, 2013, **138**, 214101–214109.
- 24 J. M. Brader and M. Schmidt, *The Journal of Chemical Physics*, 2013, **139**, 104108–104114.
- 25 C. P. Royall, J. Dzubiella, M. Schmidt and A. van Blaaderen, *Phys. Rev. Lett.*, 2007, **98**, 188304.
- 26 A. Malijevský and A. J. Archer, *The Journal of Chemical Physics*, 2013, **139**, 144901–144913.
- 27 M. Krüger and J. M. Brader, *EPL (Europhysics Letters)*, 2011, **96**, 68006.
- 28 F. Penna, J. Dzubiella and P. Tarazona, *Phys. Rev. E*, 2003, **68**, 061407.
- 29 A. J. Archer, M. J. Robbins and U. Thiele, *Phys. Rev. E*, 2010, **81**, 021602.
- 30 F. Penna and P. Tarazona, *The Journal of Chemical Physics*, 2003, **119**, 1766–1776.
- 31 L. Almenar and M. Rauscher, *Journal of Physics: Condensed Matter*, 2011, **23**, 184115.
- 32 J. Dzubiella and C. N. Likos, *Journal of Physics: Condensed Matter*, 2003, **15**, L147.
- 33 W. A. Curtin and N. W. Ashcroft, *Phys. Rev. A*, 1985, **32**, 2909–2919.
- 34 M. B. Jackson, *Molecular and Cellular Biophysics*, 1st edn., 2006.
- 35 C. Mattisson, P. Roger, B. Jnsson, A. Axelsson and G. Zaccchi, *Journal of Chromatography B: Biomedical Sciences and Applications*, 2000, **743**, 151 – 167.
- 36 Y. Li, Z. Zhang, H. P. van Leeuwen, M. A. Cohen Stuart, W. Norde and J. M. Kleijn, *Soft Matter*, 2011, **7**, 10377–10385.
- 37 D. I. Devore and G. S. Manning, *Biophys. Chem.*, 1978, **2**, 42.
- 38 N. Welsch, J. Dzubiella, A. Graebert and M. Ballauff, *Soft Matter*, 2012, **8**, 12043–12052.
- 39 O. Annunziata, D. Buzatu and J. G. Albright, *Langmuir*, 2005, **21**, 12085–12089.
- 40 D. Brune and S. Kim, *Proc. Natl. Acad. Sci. USA*, 1993, **90**, 3835–3839.
- 41 M. Lundqvist, J. Stigler, G. Elia, I. Lynch, T. Cedervall and K. A. Dawson, *Proceedings of the National Academy of Sciences*, 2008, **105**, 14265–14270.
- 42 L. Vroman and A. Adams, *Surface Science*, 1969, **16**, 438 – 446.
- 43 S. L. Hirsh, D. R. McKenzie, N. J. Nosworthy, J. A. Denman, O. U. Sezerman and M. M. M. Bilek, *Colloids and Surfaces B: Biointerfaces*, 2013, **103**, 395 – 404.

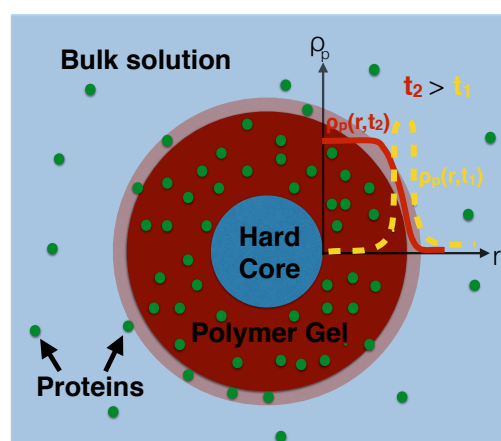


Fig. 1 Schematic representation of our system. A 60 nm hard-core PMMA nanoparticle (blue) coated with a cross-linked polymer network (hydrogel) of PNIPAM 90 nm thick (dark red) with an interface width of around 10 nm (light red). All nanoparticle dimensions are scaled with the correct size ratio (protein are represented larger than their actual size). This core-shell nanoparticle, which we also refer to as nanogel, is immersed in a protein solution (green points). Proteins are described in our DDFT model as a continuous, time-dependent radial density field $\rho_p(r,t)$ with origin at the nanoparticle's hard core / polymer boundary. Here, two density profiles corresponding to different times (yellow dashed line and, at later times, red, continuous line) are shown. Within this model, mixture of different protein types can also be easily treated.

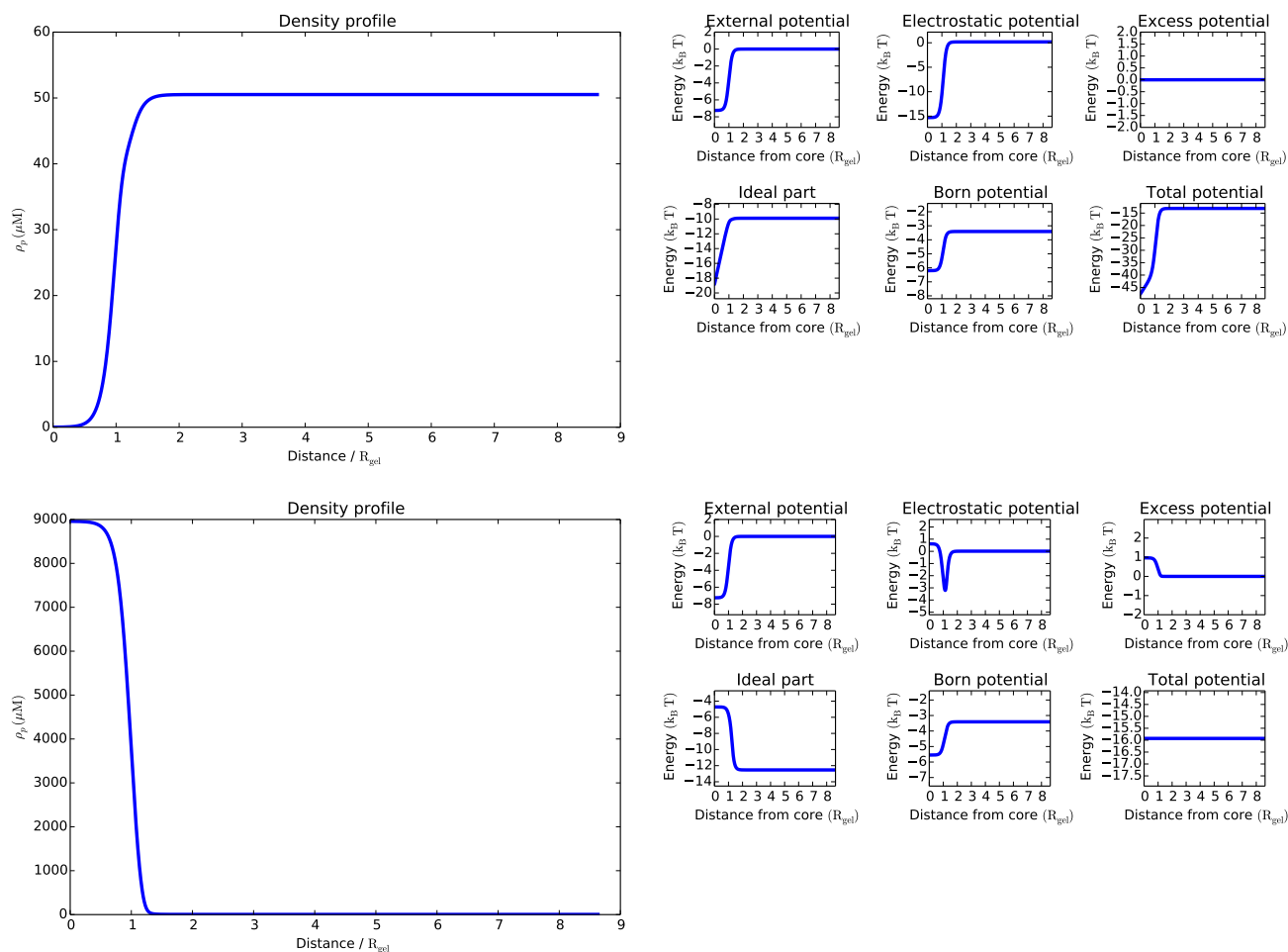


Fig. 2 Density profile and spatial variation of the different terms in the chemical potential, Eq. 8, for the initial (top) and equilibrium (bottom) density. Note that both the ideal chemical potential and the electrostatic term change slope at the gel/bulk boundary ($R=1$), hence the associated thermodynamic force must change from attractive to repulsive in the course of the simulation. Such a dynamical change in the forces driving adsorption cannot be captured with simpler models based on Langmuir kinetics, since in the latter all effects are gathered in a single equilibrium constant¹¹.

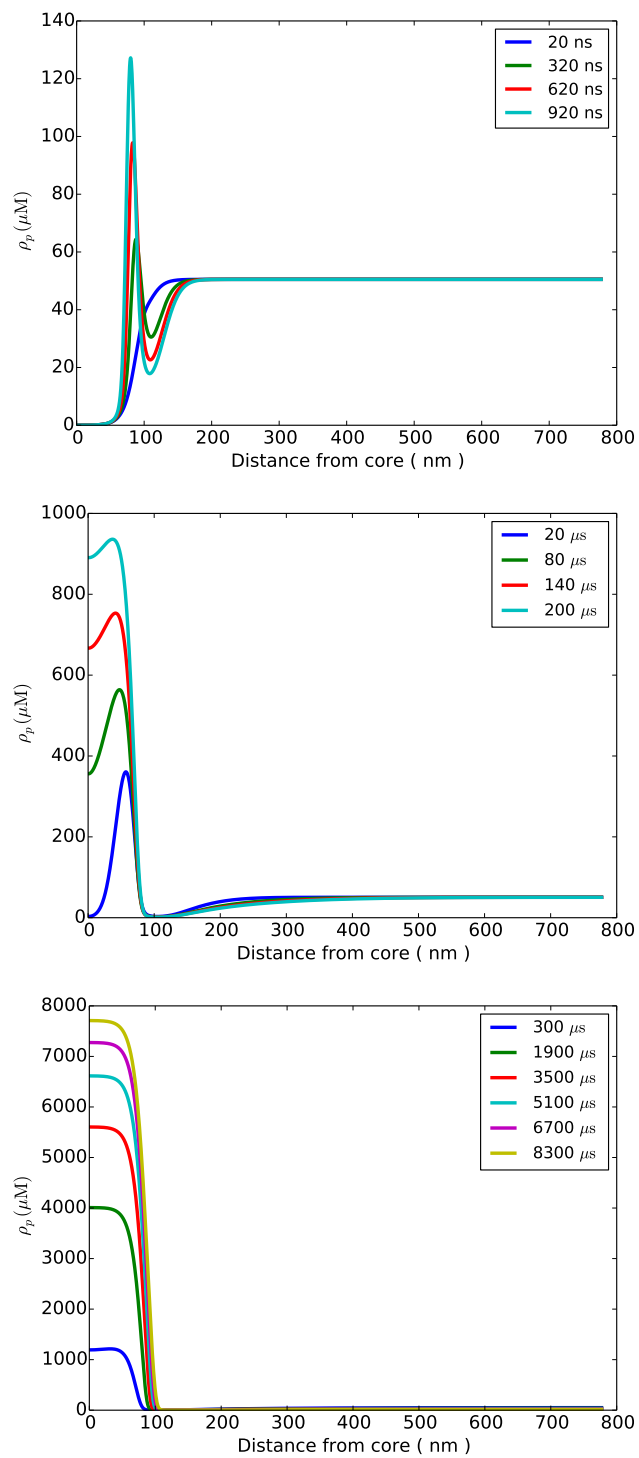


Fig. 3 Evolution of the density profile at short, intermediate and long timescales (see explanation in text).

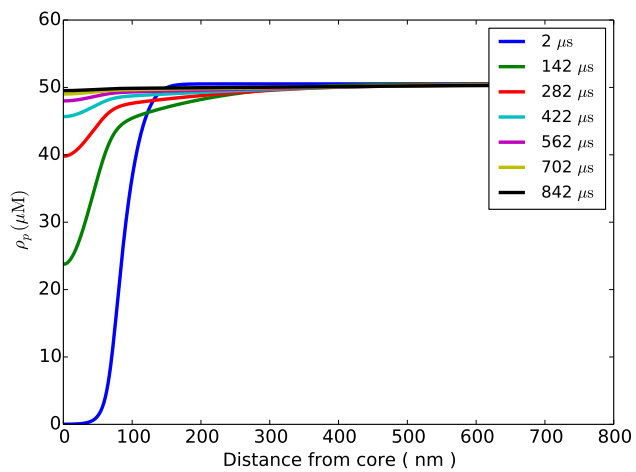


Fig. 4 Density evolution for an ideal model with spatially dependent diffusion coefficient.

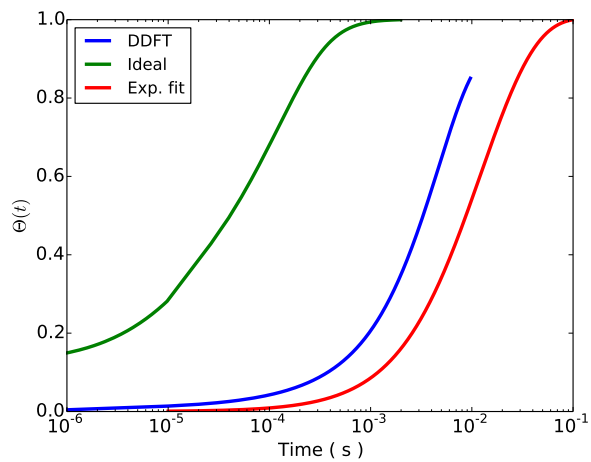


Fig. 5 Comparison of $\Theta(t) = N(t)/N(\infty)$ vs. time t for a model based on ideal diffusion, our DDFT model and for a Langmuir model fit to reproduce the experimental data in³⁸.

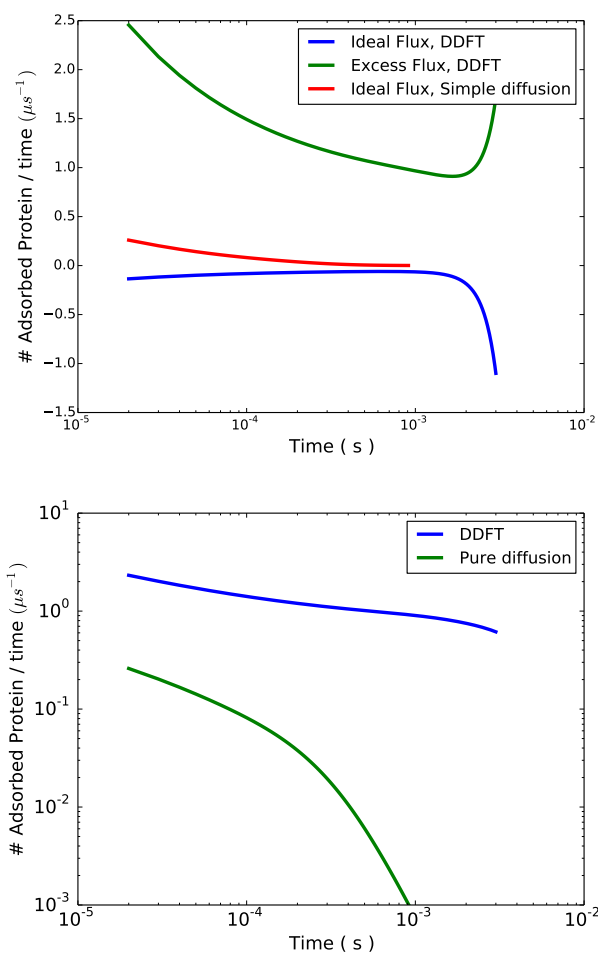


Fig. 6 Fluxes as a function of time. Top) Ideal and excess flux in our DDFT model vs ideal flux in the model of Fig. 4. Bottom) Total flux in our DDFT model and in the purely diffusive case.

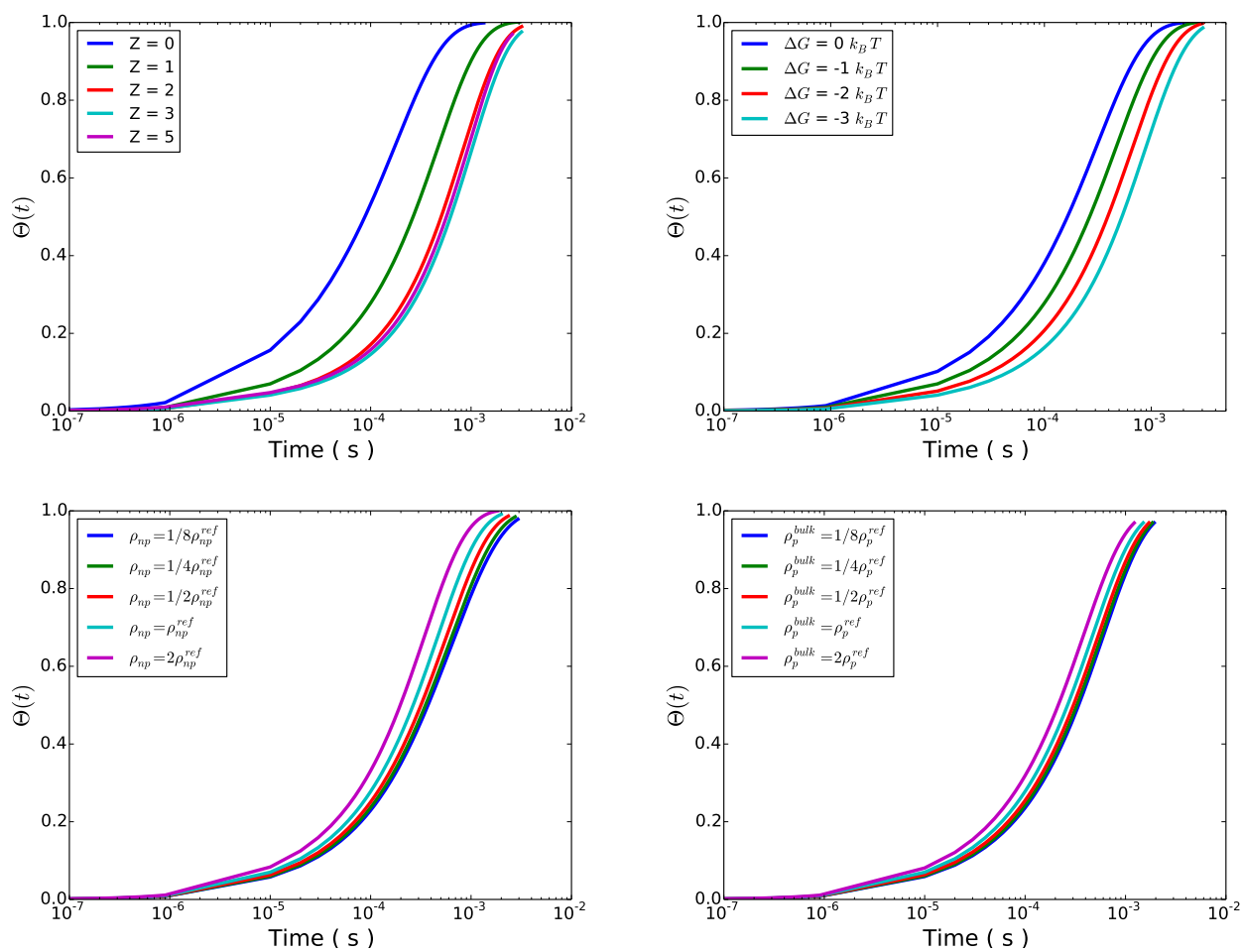


Fig. 7 Summary of simulations, loading Θ vs various parameters in our system. From top to bottom (left to write), Θ is plotted a a function of protein's valence, intrinsic adsorption energy, nanoparticles' concentration and protein concentration.

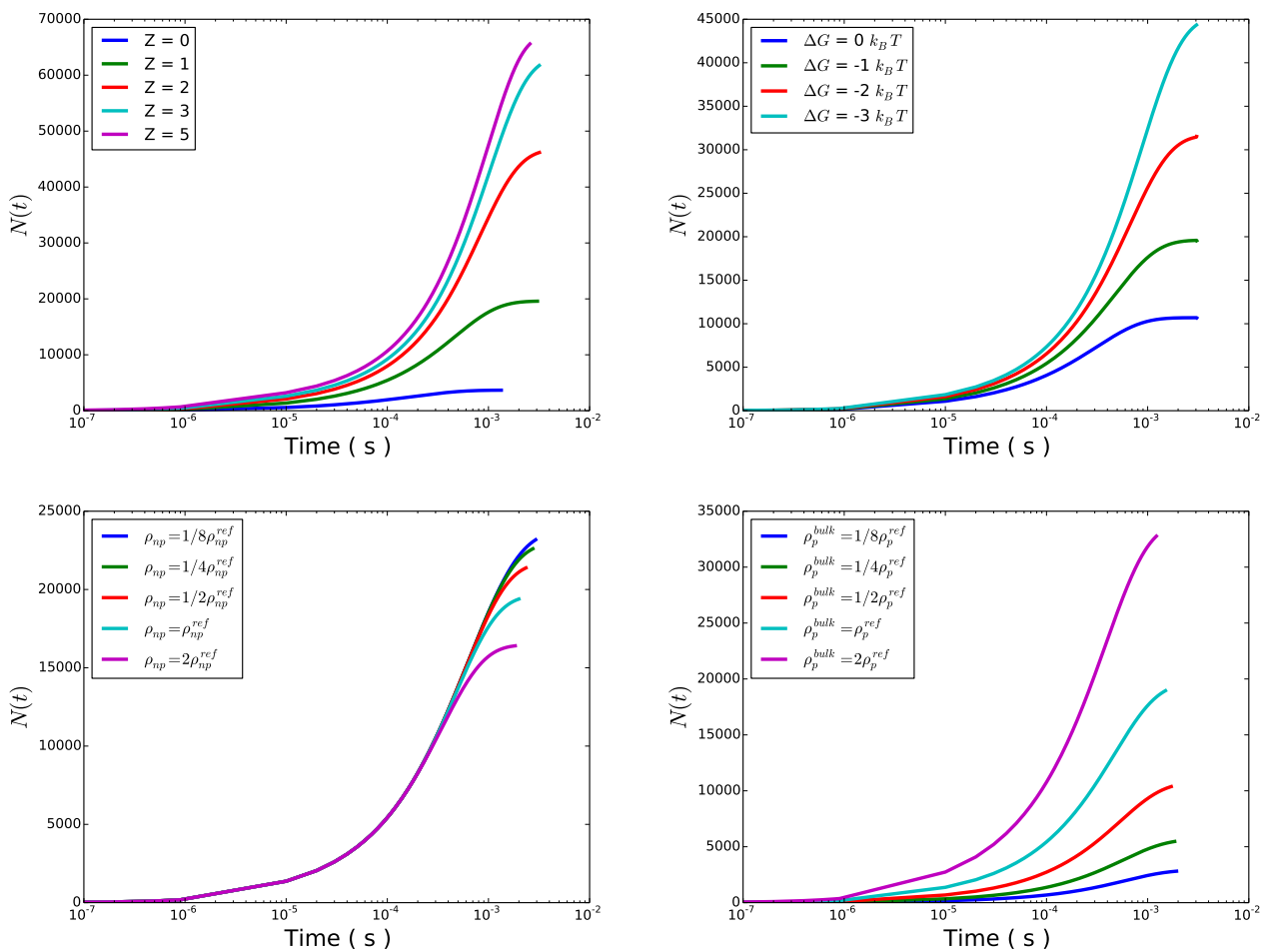


Fig. 8 As in Fig. 7, but here the un-normalised amount of adsorbed proteins is reported.